*Desalination and Water Treatment*
www.deswater.com

doi: 10.5004/dwt.2022.28295

251 (2022) 134–145
March

# Performance analysis of operating multi-stage flash distillation unit coupled with nuclear power plant

D. Harishwar[a], S.N. Amresh[a], S. Prabhakar[a], V. Murugan[b], M. Magesh Kumar[a,*]

[a]*Department of Chemical Engineering, School of Bio Engineering, SRM Institute of Science and Technology, Kattankulathur – 603 203, Tamil Nadu, India, Tel. +91 9940585262; emails: mmagesh23@gmail.com (M. Magesh Kumar), hariswarna97@gmail.com (D. Harishwar), snamresh@yahoo.com (S.N. Amresh), sivaprabha50@gmail.com (S. Prabhakar)*
[b]*Operations Head, Nuclear Desalination Demonstration Plant, BARCF, Kalpakkam, Tamil Nadu, India, email: vmgl1996@gmail.com*

Received 14 September 2021; Accepted 15 February 2022

**ABSTRACT**

Multi-stage flash (MSF) process is the most widely used technology in large scale desalination plants which utilizes low quality steam produced in nuclear power plant. The objective of this study is to analyze the performance of brine heater used in 4,500 $m^3$/d capacity MSF desalination plant at Nuclear Desalination Demonstration Plant (NDDP), Kalpakkam commissioned in 2008. The efficiency of brine heater, after 12 y of service, was investigated by analyzing the influence of volumetric flow rate and scale thickness on heat transfer rate. The tube side pressure drop increases steeply as a function of volumetric flow rate of cold fluid. A maximum pressure drop of 17.1 kPa was developed at an optimized flow rate of 1,500 $m^3$/h. The overall heat transfer coefficient increases gradually as scale thickness decreases and reached an ultimate of 4,395.3 W/$m^2$ K at a scale thickness of 0.00005 m. For small scale thickness, the percentage reduction in overall heat transfer coefficient increased steeply and attained a saturation limit at 0.00025 m scale thickness. The overall heat transfer coefficient increased from 623.4 to 646.3 W/$m^2$K as the volumetric flow rate increased from 750 to 1,500 $m^3$/h. This study shows that the thermal efficiency of brine heater has not declined significantly after prolonged years of service under different operating conditions.

*Keywords:* Multi-stage flashing, Brine heater, Heat transfer coefficient, Scale thickness, Stage number

## 1. Introduction

Multi-stage flashing (MSF) is a thermal desalination process in which heated liquid is subjected to a lower pressure to produce vapor after being flashed. MSF units are generally coupled with nuclear power plants to utilize the waste heat generated from the plants. The feed water for MSF process requires less pretreatment but produces water of high purity. Built-in energy recovery systems are used to utilize the heat to a maximum extent. The permeate produced by MSF has very high purity because the total dissolved solids concentration is in the range of 5–20 ppm. The system comprises of three sections namely heat input section which includes the brine heater, heat recovery and heat rejection sections which are coupled with the flashing modules. The system is composed of 1–10 Modules in which 1–9 Module consists of 36 stages and tenth module alone consists of 3 stages. Therefore, the system totally consists of 39 stages in which the feed is passed through all the modules. The feed (pre-treated coolant water from atomic power station which consists of nearly 35,000 ppm) passes through the 9th to 1st module after mixing with recirculation brine, where temperature of the feed is increased from 32°C to 113°C as it exits the 1st module. The feed water for

* Corresponding author.

*Presented at the Virtual International Conference on New Strategies in Water Treatment and Desalination (WTD-2021), 21–23 March 2021, by SRM Institute of Science and Technology, Kattankulathur, India*

Nuclear Desalination Demonstration Plant (NDDP) is supplied from Madras Atomic Power Station (MAPS). Both high pressure steam and low pressure steam is also provided by MAPS. The high pressure steam is used to create vacuum whereas low pressure steam is used for brine heater system. Low pressure steam generator utilizes 11.2% moist steam from high pressure turbine exhaust to produce low pressure steam which is supplied to brine heater as heating source. High pressure steam is generated by steam generating equipment to produce saturated steam at 15 kg/cm$^2$ gage pressure which is utilized in steam jet ejector to create vacuum in the whole system.

The pre-treated coolant water, consisting of 35,000 ppm total dissolved solids (TDS), from MAPS is used as feed to MSF. The main objective of pretreatment is the removal of non-condensable gases from the feed. The bicarbonates present in feed water are converted to $CO_2$ gas using hydrochloric acid treatment process. Calcium bicarbonate dissolved in feed water is treated with HCl to convert it into calcium chloride with the evolution of carbon dioxide gas. Sodium hexametaphosphate (SHMP) is added to feed water as anti-scaling agent to minimize the fouling of heating tubes. The non-condensable gases are removed from the feed using de-aerator chamber to prevent the formation of thin gas film on the surface of tubes. Otherwise the film formation will decrease overall heat transfer coefficient and reduces the quantity of heat transferred and recovered. Almost 34% of brine water desalination plant follows MSF distillation technique and this method is widely followed in the Middle East countries to minimize the salt concentration in sea water [1]. The type of brine heater used for heat input is 1,2 – shell-and-tube heat exchanger which utilizes saturated steam at 128°C as shell side fluid and brine as tube side fluid. The temperature of brine solution increases from 113°C to 121°C in the heat exchanger. The performance ratio (PR) of MSF plant depends on the number of stages. For a brine temperature of 106°C, the PR ranges between 79% and 327% [2]. The heat exchanger design algorithm developed by Kern was used to calculate the design variables for brine heater. Heat duty, area of heat transfer, number of tubes, and velocity of tube side fluid, individual heat transfer coefficient for shell side and tube side, overall heat transfer coefficient and tube side pressure drop was calculated using the design algorithm proposed by Kern. The thermo-economic optimization of shell and tube heat exchanger depends on mass flow rate recovery [3]. Different tube geometries and configurations are used to improve the heat transfer coefficient on the shell side and tube side of heat exchanger. The shell side heat transfer coefficient is enhanced by rotational motion of twisted circular tube because secondary flow is induced and boundary layer is destroyed [4]. A generalized disjunctive programming (GDP) model was developed for the optimization of shell and tube heat exchanger to minimize the total capital cost. This model involves with selection of four tube-side techniques and three shell-side techniques for design optimization [5]. Shell-and-tube heat exchangers are widely used in organic Rankine cycle (ORC) systems. The purchased cost and exergy loss of heat exchanger is affected by the factor whether the organic fluid flows either through inside or outside the tubes [6]. The total heat transfer rate and pressure drop along a shell and tube heat exchanger depends on segmental porous baffles and baffle cut. A considerable amount of pressure drop is produced when low baffle cuts are used but low baffle cuts provide the highest heat transfer rate [7].

A steam jet ejector used in MSF unit at NDDP plant is used for both vacuum generation and de-aeration purpose. The constant pressure model was used to design the steam jet ejector based on the assumptions: isoentropic expansion of motive steam occurs in nozzle and isentropic compression of mixture occurs in diffuser section, both motive steam and entrained vapors are completely saturated, flow in ejector follows adiabatic condition and at steady state. The major design parameters calculated using algorithm for steam jet ejector are saturation temperature, compressed vapor pressure, throat area of nozzle and ratio of areas of the nozzle throat to the nozzle outlet. For the design and rating of steam jet ejectors semi-empirical models are developed to express the entrainment ratio as a function of the expansion ratio. The motive steam pressure at the nozzle exit as a function of the evaporator and condenser pressure admits the complete design aspects of ejector [8]. The efficiency of ejector depends on the mechanism of fluid flow and heat transfer. The entrainment ratio, pressure lift ratio and the performance rests on nozzle position. The optimal nozzle position guarantees for minimum friction losses and kinetic energy losses [9]. Computational fluid dynamics (CFD) technique is applied to analyze the influence of mixing chamber geometry on the performance of steam jet ejectors. The optimum length and convergence angle of mixing chamber affects the internal flow characteristics of steam ejector [10]. Pressurized vapor is used as motive flow in steam ejectors for running in steam cycles. The thermal energy consumption is mainly affected by motive fluid flow pressure [11]. The fluid flow dynamics in the primary nozzle of steam ejector is modeled either based on ideal gas modeling or wet steam modeling. The ejector primary nozzle is simulated for different values of area ratios. The nozzle static pressure obtained using wet steam simulation is higher than value obtained using ideal gas model. The nozzle momentum flux for both ideal gas and wet steam models are almost same except near to the nozzle throat where nucleation occurs [12]. The performance of steam ejector depends primarily on three geometrical factors namely the area ratio between the nozzle and constant area section, nozzle exit position and constant area section length. The optimal area ratio depends on operating conditions. The flow rate in the primary nozzle is fine-tuned by providing a spindle like arrangement in the primary nozzle [13]. A model based on perturbation procedure of linearized and axisymmetric supersonic flow is used to evaluation of the entrainment ratio of double choked ejectors. The developed model is applicable for the three regions namely: primary flow nozzle, secondary flow channel and region of interaction between the supersonic nozzle jet and the secondary flow. The model entrainment ratio deviated from experimental data in the order of 7% [14].

The performance ratio of MSF unit depends on flashing temperature range and magnitude of heat transfer coefficient. A comparative study between once through long tube (MSF-OT-LT) with atmospheric deaerator, and brine recycle cross tube (MSF-BR-CT) evaporators concludes that the heat transfer area of MSF-OT-LT system is 34% lesser

than MSF-BR-CT system. The lower friction loss in the tubes reduces the pumping power of the MSF-OT-LT system by 40% [15]. A comparative study between MSF once through (MSF-OT) system and MSF-OT combined with thermal vapor compression (MSF-OT/TCV) indicates that the thermal performance ratio of the process was affected by vapor entrainment and compression in different stages. An increased thermal performance ratio, between 42% and 57%, was observed for MSF-OT/TCV configuration over the conventional MSF-OT configuration [16]. The design of MSF brine circulation (MSF-BC) system was performed using mass balance, energy balance, and heat transfer and performance parameters equations. For a temperature difference of 4.5°C per stage the distilled water produced is 131.42 ton/h utilizing a heat transfer area 5,154.2 $m^2$. The design criteria for MSF-BC unit have successfully met the water requirement of steam power plant [17]. The mathematical model for MSF process elucidates the relationship between fluid flow rate, temperature of fluids, surface area for heat exchange and rate of brine recirculation. The model equations are developed based on the assumptions such as constant heat transfer surface area and dynamic variation of water physical properties with operating temperature and salinity [18]. ChemCAD simulator program is most suitable to develop steady state desalination process. The simulation results obtained from this model matches with actual industrial data [19]. The yield of MSF plant depends mainly on the number of stages and quantity of fuel used for heat recovery and boiler section. Approximately 1.2 L of fuel is required per 3,785 L of water produced [20]. The thermal efficiency of MSF unit is increased by retrofitting the existing plant setup to utilize solar power. As a result of this 17.8 MW of fossil energy is conserved by using the thermal energy from solar radiation. The steam consumption used for heating the brine water is minimized [21]. The energy requirement in MSF plant is reduced by integrating with thermal vapor compressor. The thermal performance efficiency for this integrated system rises from 8.58% to 12.96% and a 33% reduction in steam consumption is achieved. The energy consumption per unit mass of pure water produced is reduced [22]. In general the heat exchange capacity of brine heater slackens after it was used continuously because of scale formation, stress related mechanical failures and corrosion issues. An analysis of thermal efficiency of heater, after prolonged years of service, is very important from energy-economy conservation point of view. The result of this analysis helps to schedule maintenance activities, repair and replacement of faulty heat exchanging equipment. The literature analysis reveals that the working efficacy of brine heater which was under prolonged use under different operating conditions was not examined so far. Furthermore the studies conducted so far have recommended using integrated system for energy conservation and management in thermal desalination process. Hence this work is carried out is to analyze the working efficiency of existing brine heater in the desalination plant after decades of service. An attempt has been made in this study to analyze the performance of operating brine heater in MSF plant. The efficacy of brine heater is tested by analyzing the influence of volumetric flow rate and scale thickness on overall heat transfer coefficient. A brine heater design algorithm based on Kern method is used to design a brine heater theoretically and the equations are solved using MS Excel software package. The results obtained from MS-Excel simulation is compared with the data collected from the actual brine heater in the plant.

## 2. Preface to the desalination plant under study

The Nuclear Desalination Demonstration Plant (NDDP) located at Kalpakkam (near Chennai), Tamil Nadu, India is the world's largest hybrid seawater desalination plant coupled to an existing nuclear power plant. The NDDP plant has a total production capacity of 6,300 $m^3$ potable water/d from seawater. Out of this total water produced, the MSF plant contributes 4,500 $m^3$/d and the remaining 1,800 $m^3$/d is produced by reverse osmosis process. The desalination process in a MSF plant utilizes low grade steam from the nearby nuclear power plant as source of energy. The distilled water produced in this plant is mainly used for drinking purpose and for cleaning of accessories in nuclear plant. NDDP is set up by Department of Atomic Energy, Government of India adjacent to Madras Atomic Power Station (MAPS) primarily to utilize the low quality steam produced from the turbine of MAPS. The construction, operation and maintenance of NDDP at Kalpakkam was undertaken by Bhabha Atomic Research Centre (BARC), Trombay based on the past operational experience of MSF and reverse osmosis plant at Trombay. The desalination plant at NDDP is a hybrid type which couples MSF-RO process to produce 6,300 $m^3$/d distilled water. The NDDP plant is coupled to 2 × 170 MWe pressurised heavy water reactors at the Madras Atomic Power Station (MAPS), Kalpakkam.

In this MSF plant, the boiling point of water is increased up to 121°C by raising the pressure of water by 2 bar. The superheated water is then allowed to cool at the rate of 2°C drop per stage for all the 39 stages, and the cooled water is allowed to flash evaporate and condense as pure water at reduced pressure condition. In 2012, the cost of producing distilled water using MSF technology is 10 paisa per litre, and 6 paisa per litre in the case of reverse osmosis. The cost of power consumed, steam utilized, chemicals procured, maintenance and annual depreciation accounts for the production cost in MSF plant. The MSF desalination process plant has three distinct sections namely the heat rejection section, the heat recovery section and the heat input section (i.e., brine heater). Fig. 1 shows a typical schematic diagram of the MSF desalination plant under consideration in this study. In this plant the seawater gets heated up as it is passed through tube bundle of the heat reject section. A portion of this heated brine water is treated with chemicals to enhance the quality and to use as process feed. The brine from the last reject stage is recycled and passed through tube bundles of the heat recovery section where it is heated by the condensation of the flashing brine in the stages. The brine is then further heated up in the brine heater to a maximum of 121°C by steam in the brine heater, which is the heat input section of the plant. The hot brine from the heater outlet is then fed to first stage of the recovery section. The first stage is maintained at a pressure, which is slightly below the saturation pressure corresponding to 121°C. As a result the brine flashes in order to attain equilibrium with the

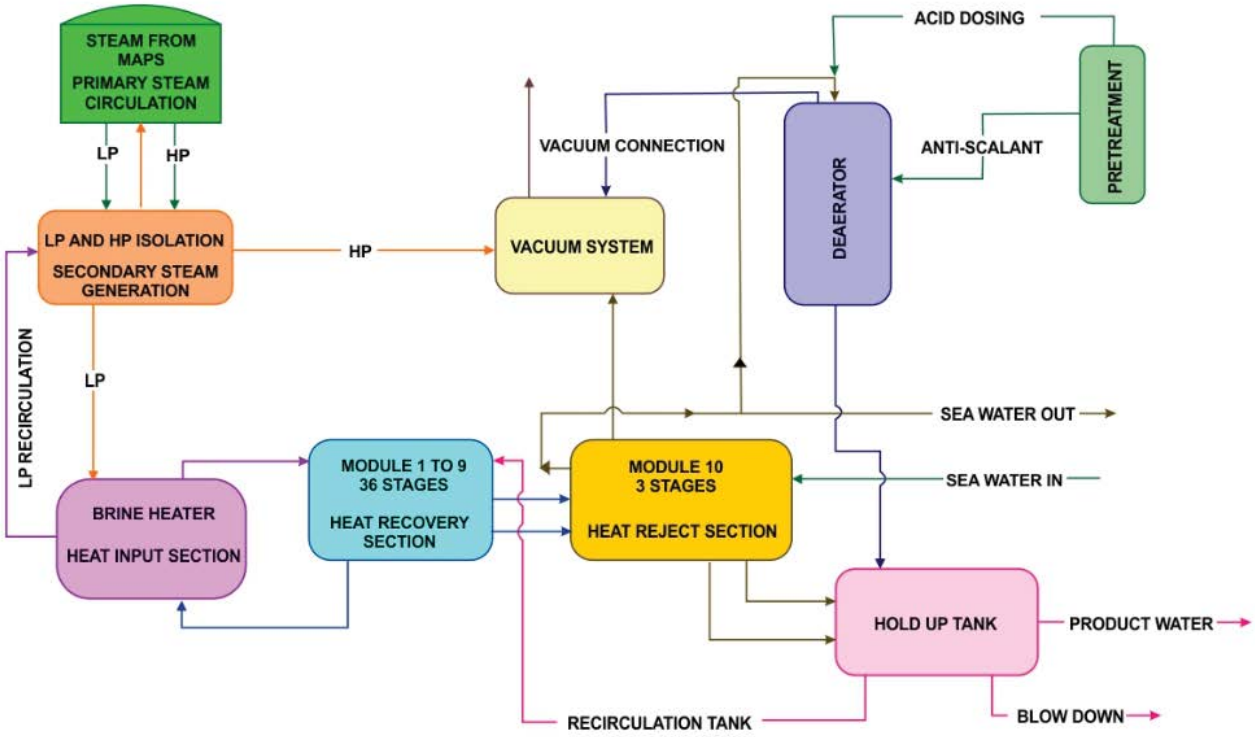


Fig. 1. Schematic process flow sheet for MSF plant under study.

prevailing pressure. The vapor so formed is condensed on the outside of the tube bundle (through which the re-circulating brine is flowing) forming distillate. When compared with standalone desalination plants, the energy consumption in MSF process coupled with nuclear power plant is reduced by about 50% but it is still considered as one of the energy intensive process. A detailed thermal analysis for MSF plant is necessary to under the process economics and identifying the optimal values of process parameters.

There are four major components namely tube bundle, product tray, brine pool and vapor space are present in any stage of MSF plant. The brine solution initially flashes from brine pool, then condenses on the tube bundle and finally collected in the product tray. The brine entering to next stage flashes to reduce its temperature to equilibrium with stage pressure because the next stage is at lower pressure. Similarly, distillate flowing in the product tray also re-flashes to achieve vapour – liquid equilibrium. The distilled water from last reject stage is pumped out as product. MSF process plant comprises of three sections namely heat input section (includes brine heater), heat recovery and heat rejection sections which are coupled with the flashing modules. The system considered in this study consist of 1–10 modules in which 1–9 module consists of 36 stages and 10th module alone consists of 3 stages. Therefore, the MSF system under study totally consists of 39 stages in which the feed is passed through all the modules. The feed (pre-treated coolant water from MAPS which consists of nearly 35,000 ppm) passes through the 9th to 1st module after mixing with recirculation brine, where temperature of the feed is increased from 32°C to 113°C and finally exit from the first module. The exhaust steam from MAPS is the primary source for low pressure (LP) steam and high pressure (HP) steam for MSF plant. The HP steam is used to create vacuum for the whole system because this system works under the principle of flashing (heating the liquid by reducing the pressure at isothermal conditions). The LP steam is primarily used for brine heater. This is produced by LP steam generator which utilizes 11.2% moist steam from HP steam generating turbine exhaust unit after passing through moisture separator to produce saturated steam at 128°C which is supplied to brine heater. HP steam is generated by HP steam generating equipment using 0.2% moist steam at 40 kg/cm$^2$ abs steam line to the hogging ejector at MAPS, which produces saturated steam at 15 kg/cm$^2$ gauge which is supplied to the steam jet ejector. The pre-treatment of feed is done by acid dosing method to minimize the dissolved solids and suspended solids concentration of coolant water emerging from MAPS.

De-aerator is used to remove non-condensable gases from the feed. These gases are removed because they form film-like layers on the outer surface of tubes thereby increasing heat transfer resistance. In view of this the amount of heat transferred and heat recovered is reduced. The de-aerator unit is maintained at a pressure of 0.94 kg/cm$^2$ to execute this process. A two-stage steam jet ejector is used for vacuum generation as well as for de-aeration purposes. A motive steam of pressure 15 kg/cm$^2$(abs) is utilized in the steam jet ejector. In the first stage 240 kg/h of steam is utilized and to the second stage 270 kg/h of steam is employed. The ejector generates a suction pressure of 0.06 kg/cm$^2$ (abs) for water vapor load of 225 kg/h and non-condensable gas load of 60 kg/h. The brine heater is used as heat input source

for MSF plant. The heat exchanger type used is 1,2 shell-and-tube heat exchanger with saturated steam at 128°C as shell side fluid and brine solution as tube side fluid. In this operation the latent heat of steam is exchanged to relatively cold brine solution. Because of this, the brine solution flowing inside the tubes is heated from 113°C to 121°C. The material of construction for the shell is carbon steel and the tubes are made with Cu-Ni (90:10) to provide high heat transfer and prevent deleterious corrosive effects of scaling impurities. The brine heater has 2,160 tubes each of length 4.5 m, 19 mm outer diameter and thickness 1.25 mm. The brine heater is insulated with a jacket to prevent heat loss to the surroundings. The flashing chamber consists of a orifice submerged in brine pool, demisters, tube bundle and distillate tray. The size of the submerged orifice can be varied to control the flow rate inside the chamber. After the vapors are flashed from the surface, they make use of the latent heat required from the bulk of the brine itself, cooling down the solution and the demisters which is made of meshed pads and the support is used to remove the entrained brine fluid vapor droplets from the vapor is which is being flashed. This is necessary to reduce the salinity of the product and to reduce scaling. The condensation occurs on the outer surface of the tubes and the steam loses its latent heat to the feed seawater which consequently gets heated up. Hence a major fraction of the heat energy is recovered and retained this process.

## 3. Modeling basis for brine heater and steam jet ejector

Based on energy balance and mass balance for brine heater, numerous steady state mathematical models have been developed to exhibit a functional relationship between the design variables and different operating conditions. Kern design procedure and equations are used in this study to evaluate the thermo-hydraulic performance of a heat exchanger. This method is most suitable for the "rating program" of a heat exchanger because it determines heat flux, rate of heat transfer rate and temperatures of outlet stream for specified inlet fluid flow rates, inlet temperatures, and the pressure drop for an existing heat exchanger. Kern method is simple to apply because the calculation steps in this procedure are analogous to equations for flow in circular tubes. In a brine heater the temperature of re-circulating brine increases due to heat of condensation of inlet steam. This re-circulating brine enters the heater from the first stage of the heat recovery section. The tube flowing through the tubes are heated up by the condensation of steam on the outside surface of exchanger tubes. For a brine heater, the mathematical models are developed based on heat balance for tubes and heat balance for brine solution. The model studies the dynamic variation of tube wall temperature and brine solution temperature as a function of time. The variables such as enthalpy of steam, enthalpy of saturated solution, heating surface area, heat capacity and flow rate of streams influences the heat flux and temperature of brine solution. The design variables for a brine heater are calculated using Kern method in Microsoft Excel office software package. The MSF simplified model is used in this study to assess the system performance and to acquire design parameters. This model assumes constant heat capacity for all liquid streams, uniform temperature drop across each stage for flashing brine and feed sea water and negligible effect of non-condensable gases on heat transfer process. The following mathematical equations are proposed for MSF simplified model:

Overall material balance equation is defined by:

$$M_f = M_d + M_b \tag{1}$$

where $M_f$ (kg/s), $M_d$ (kg/s) and $M_b$ (kg/s) is mass flow rate of feed seawater, distillate and brine respectively.

Component mass balance based on salinity concentration is

$$X_f M_f = X_b M_b \tag{2}$$

where $X_f$ and $X_b$ is the mole fraction of salt in feed and brine respectively.

Assuming a linear temperature distribution for the flashing brine and the seawater flowing inside the condenser tubes, the number of stages ($n$) is calculated using:

$$n = \frac{\left(T_o - T_n\right)}{\Delta T} \tag{3}$$

where $T_o$ (°C) is temperature of brine leaving the preheater and $T_n$ (°C) is temperature of brine leaving the last stage.

Condenser temperature in stage '$i$' is calculated using:

$$t_i = T_f + \left(n - \left(i - 1\right)\right)\Delta t \tag{4}$$

where $T_f$ (°C) is temperature of feed seawater.

Using the principle of conservation of energy in each stage, the amount of flashing vapor formed in stage '$i$' is calculated as:

$$D_i = M_f y\left(1 - y\right)^{(i-1)} \tag{5}$$

where $y$ is the specific ratio of sensible heat to latent heat and $M_f$ is defined already in Eq. (1).

Application of energy balance for recirculating brine and heating steam yields the model equations for tube wall and for brine solution.

Heat balance for tube is defined by:

$$\frac{\partial T_{W,1}}{\partial t} = \frac{\alpha WS\left(E_{S,1} - E_{L,1}\right) - h_1 A_1\left(T_{W,1} - T_{D,1}\right)}{C_T W_{T,1}} \tag{6}$$

Heat balance for brine solution is expressed as:

$$\frac{\partial T_{B,i}}{\partial t} = \frac{\alpha h_1 A_1\left(T_{W,1} - T_{D,1}\right)}{C_B W_{\mathrm{RS1}}} - \frac{W_{R1}\left(T_{B,1} - T_{C,1}\right)}{W_{\mathrm{RS1}}} \tag{7}$$

where $T_W$ (°C) is tube wall temperature, $W$ (kg/s) is amount of water produced, $S$ (kg/s) is mass flow rate of steam, $E_L$ (J/kg) is enthalpy of saturated liquid, $E_S$ (J/kg) is enthalpy of saturated steam, $C_T$ (J/kg K) is specific heat of tube material, $h_1$ (W/m$^2$ K) is convective heat transfer coefficient and

$W_{R1}$ (kg/s) is flow rate of brine from stage 1. Eqs. (6) and (7) are solved simultaneously using fourth order Runge–Kutta method to obtain the temperatures $T_W$ and $T_B$, respectively.

Scale formation and fouling of equipment has detrimental influence on the performance of MSF plants. Sea water contains dissolved salts and finely suspended solids which is responsible for scale deposits and tube fouling. The major scale forming compounds in sea water mainly includes calcium carbonate, calcium sulfate and silica. The precipitation of calcium carbonate scale is favored at elevated temperature and decreased level of carbon dioxide concentration. The scale formation due to calcium sulfate is most likely to occur at high temperatures. Severe scaling may occur if the ionic concentration of calcium and sulfate exceeds the saturation solubility limit in the feed sea water. Silica scaling occurs at high temperature and higher concentrations. The influence of silica scaling is prevented by maintaining its aqueous phase concentration below the saturation limit. Scale deposit on one side or both sides of the tubes provide extra resistances to heat flow and reduce the overall heat transfer coefficient and rate of heat transfer. The effect of scale deposit on heat transfer rate is accounted by adding a term $1/(dA{\cdot}h_d)$ to the standard form heat exchanger equations. If scale formation is assumed to occur on both inside and outside surface of the tubes, the overall temperature drop across the tube is defined by the expression,

$$\Delta T = dq\left(\frac{1}{dA_i h_{\mathrm{di}}}+\frac{1}{dA_i h_i}+\frac{x_w}{d\overline{A_L}k_m}+\frac{1}{dAA_o h_o}+\frac{1}{dA_o h_{\mathrm{do}}}\right) \tag{8}$$

where $k_m$ (W/m K) is thermal conductivity of tube material, $x_w$ (m) is tube wall thickness, $d\overline{A_L}$ (m$^2$) is logarithmic mean area and $h$ (W/m$^2$ K) is the heat transfer coefficient.

The conventional steam jet ejector has three main parts namely the nozzle, the suction chamber and the diffuser. Two models namely, constant pressure model and constant area model, are developed to analyze the performance of steam jet ejector. The models are categorized based on the methodology of mixing the motive steam and entrained vapor. Literature survey reveals that the design models of stream mixing at constant pressure are more widely followed common in literature because the performance of the ejectors designed by constant pressure model is more superior to the constant area method. Also the simulated results from constant pressure model very well match with the experimental data. The model equations developed for a steam jet ejector is based on overall material balance, entrainment ratio, compression ratio, expansion ratio, Mach number calculation, pressure lift in the diffuser and the area ratio of the nozzle throat and diffuser constant area. The model equations for designing brine heater and steam jet ejector are explained in section 4 in this study.

## 4. Design algorithm for brine heater and steam jet ejector

The brine heater was designed using the Kern method which correlates data for standard exchangers by a simple equation similar to expressions for fluid flow in pipes and tubes. However, this method is applicable only to fixed baffle cut (25%) and cannot adequately account for leakages in baffle-to-shell and tube-to-baffle. The design procedures for 1,2 shell-and-tube heat exchanger was carried out in Microsoft excel package. The design formulas and equations are fed into Microsoft excel office software and the brine solution inlet and outlet temperature was used as preliminary input data for subsequent calculations. All the thermo-physical properties were calculated at the mean temperature of fluid. An energy balance equation is used to calculate the heat duty.

$$Q = mC_p\Delta T \tag{9}$$

where $Q$ (J/s) is heat duty of brine heater, $m$ (kg/s) is the mass flow rate of brine and $\Delta T$ (K) is the temperature difference inlet temperature and outlet temperature of brine solution. The heat exchange area is calculated using:

$$A = \frac{Q}{U\cdot \mathrm{LMTD}} \tag{10}$$

where $A$ (m$^2$) is the surface area available for heat transfer, $U$ (W/m$^2$ K) is the overall heat transfer coefficient and LMTD (K) is log mean temperature difference. The total number of tubes is calculated with:

$$n_t = \frac{A}{\pi\cdot d_o\cdot L} \tag{11}$$

where $n_t$ is number of tubes necessary for achieving desired thermal efficiency, $d_o$ (m) is the tube outer diameter and $L$ (m) is the length of tube. The velocity of tube side fluid is calculated using:

$$V_t = \frac{4m\left(n_p/n_t\right)}{\pi\cdot d_i^2\cdot \rho_t} \tag{12}$$

where $m$ (kg/s) is the mass flow rate of fluid, $n_p$ is number of tube passes, $n_t$ is number of tubes, $d_i$ is the inner diameter of tube and $\rho_t$ is tube side fluid density. The heat transfer coefficient for the shell-side in the Kern Method can be estimated from:

$$h_s = \left(\frac{0.36k_s}{D_e}\right)\mathrm{Re}_s^{0.55}\,\mathrm{Pr}_s^{1/3} \tag{13}$$

where $k_s$ (W/m K) is the thermal conductivity of shell-side fluid, $\mathrm{Re}_s$ is the Reynolds number for the shell-side, $\mathrm{Pr}_s$ is the Prandtl number for the shell-side fluid and $D_e$ is the equivalent diameter on the shell-side. For fully developed turbulent flow in tubes the heat transfer coefficient is calculated using Dittus-Boelter correlation which is defined by the expression.

$$h_t = \frac{0.023\left(\mathrm{Re}_t\right)^{0.8}\left(\mathrm{Pr}_t\right)^{0.33}K}{d_i} \tag{14}$$

where $K$ (W/m K) is thermal conductivity of tube material. The pressure drop due to friction is calculated using the expression:

$$\Delta P_f = \frac{f \cdot G_t^2 \cdot L \cdot n}{2\rho_t d_i} \tag{15}$$

where $\Delta P_f$ ($Nm^{-2}$) pressure drop due to friction, $f$ is the tube side friction factor, $G_t$ (kg/s) is mass flow rate of tube side fluid, $L$ (m) is length of the tube, $n$ is number of tube passes and $d_i$ (m) is inner diameter of the tube. The pressure drop due to change in direction of tubes is evaluated by:

$$\Delta P_t = \frac{4 \cdot n \cdot V_t^2 \cdot \rho_t}{2} \tag{16}$$

where $V_t$ ($ms^{-1}$) is tube side fluid flow velocity and $\rho_t$ ($kg/m^3$) is the density of tube side fluid.

In the present study, the steam jet ejector in MSF section is used for vacuum generation and de-aeration. The algorithm based on constant pressure model was used for the design of steam jet ejector. The model equations used to design a steam jet ejector is defined as in [23].

Overall material balance:

$$m_p + m_e = m_c \tag{17}$$

where $m_p$, $m_e$ and $m_c$ is the mass flow rate (kg/s) of primary steam, entrained vapor and compressed vapor mixture respectively.

$$\text{Entrainment ratio} = \frac{m_e}{m_p} \tag{18}$$

$$\text{Compression ratio} = \frac{P_c}{P_e} \tag{19}$$

where $P_c$ is compressed vapor pressure (Pa) and $P_e$ is the pressure of entrained vapour.

Mach number is used to explain the isentropic expansion of the primary fluid in the nozzle region.

$$M_{P2} = \sqrt{\frac{2\eta_n}{\gamma - 1}\left[\left(\frac{P_p}{P_2}\right)^{(\gamma-1/\gamma)} - 1\right]} \tag{20}$$

where $M$ is the Mach number, $P$ (Pa) is the pressure, $\gamma$ is the isentropic expansion coefficient and $\eta_n$ is the nozzle efficiency.

The saturation temperatures are calculated using the correlation:

$$T = \left(42.6776 - \frac{3{,}892.7}{\left(\ln\left(P/1{,}000\right) - 9.48654\right)}\right) - 273.15 \tag{21}$$

where $P$ (kPa) is saturation pressure. The nozzle throat area is defined by the expression:

$$A_1 = \frac{m_p}{P_p}\sqrt{\frac{RT_p}{\gamma\eta_n}\left(\frac{\gamma+1}{2}\right)^{(\gamma+1)/(\gamma-1)}} \tag{22}$$

where $m_p$ (kg/s) is mass flow rate of motive steam, $\gamma$ is isentropic expansion coefficient and $\eta_n$ is the nozzle efficiency.

The area ratio of the nozzle throat and the nozzle outlet is defined by the expression:

$$\frac{A_2}{A_1} = \sqrt{\frac{1}{M_{P2}^2}\left(\frac{2}{\gamma+1}\left(1 + \frac{(\gamma-1)}{2}M_{P2}^2\right)\right)^{(\gamma+1)/(\gamma-1)}} \tag{23}$$

where $A_2$ is the area of the nozzle outlet.

The steady state performance of MSF plant is judged by the key parameters namely salinity ratio (SR) and gained output ratio (GOR). SR is defined as the ratio between TDS in circulated brine water and TDS in sea water whereas the GOR is the ratio between mass flow rate of product water and mass flow rate of steam. For the MSF plant under study the mass flow rate of distilled water is 52.08 kg/s and steam flow rate is 6 kg/s. The GOR at steady state operating condition is 8.68 which indicate that the MSF plant is working efficiently.

## 5. Results and discussion

The model equations for designing a brine heater are defined in Eqs. (9)–(16). These equations are simulated using MS Excel built-in algorithms and functions and a comparison of model results with plant data's are presented in Table 1. The validity of Kern design equations and simulation results are tested by analyzing the % error between model predicted value and actual plant data. In all the observed cases, the simulated results matches with actual data collected in MSF unit. The % error is less than 5% which is in the tolerable limit and also confirms the prediction ability of design equations. The design algorithm depicted in Fig. 2 explains the major design variables required and calculated variables for a steam jet ejector. The input variables such as entrainment ratio, mass flow rate of compressed vapor mixture, pressure of compressed vapor, entrained vapor pressure, motive steam pressure, isentropic expansion coefficient, efficiencies of the nozzle and diffuser. The stream temperatures are calculated using the standard equations. Using these stream temperatures as input variables, the flow rate of motive steam and entrained vapor is calculated using the design equation. The cross section area of ejector and area ratio is calculated using previous block output variables. The simulated design variables for single stage steam jet ejector are reported in Table 2. The design equations defined in Eqs. (17)–(23) are solved using MS Excel default mathematical functions. The nozzle area at the throat and at the outlet are obtained as $3.38 \times 10^{-3}$ $m^2$ and $8.39 \times 10^{-4}$ $m^2$ respectively. In Fig. 3 the effect of volumetric flow rate of cold fluid on total tube side pressure drop is reported. The tube side pressure drop increases continuously as function of volumetric flow rate. This is in accordance with the statement, the higher the flow rate through a tube the greater is the pressure drop. The pressure drop varies directly with volumetric flow rate. As the volumetric flow rate of fluid increases, the friction resistance between fluid layer close to wall and the wall surface increases. This is responsible for an increase in pressure drop as the volumetric flow rate increases. Since a tube of uniform cross section is used, an increase in volumetric

Table 1
Comparison between actual plant data and simulated values for brine heater obtained from solving the model equations using MS Excel in-built algorithms and expressions

| Parameter | Actual design variable in MSF plant | Simulated results from MS Excel package | % error |
|---|---|---|---|
| Mass flow rate of steam (kg/s) | 6 | 6.03 | 0.497% |
| Number of tubes | 2,160 | 2,168 | 0.369% |
| Overall heat transfer coefficient (W/m$^2$ K) | 2,544 | 2,485.17 | 2.37% |
| Heat duty of the brine heater (kJ/s) | 13,155 | 13,143.5 | 0.0875% |

*Note*: $\%\,\text{error} = \dfrac{\left|\left(\text{model value} - \text{experimental value}\right)\right|}{\left(\text{model value}\right)} \cdot 100.$

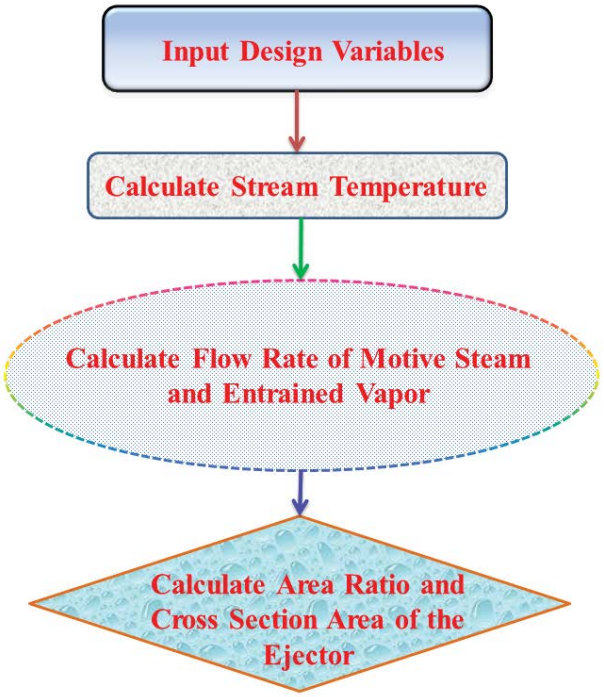


Fig. 2. Design algorithm for steam jet ejector.

flow increases the fluid flow velocity. There is a possibility of turbulent zone formation at high fluid velocity which causes the degradation of hydrodynamic boundary layer developed at low volumetric flow rate. The maximum pressure drop obtained was 17.1 kPa at a flow rate of 1,500 m$^3$/h.

The functional relationship between volumetric flow rate of cold fluid and overall heat transfer coefficient was studied and reported in Fig. 4. It was observed that as the flow rate increases, the overall heat transfer coefficient also increases for various scale thickness. It may be attributed to the shifting of flow behavior from laminar flow to turbulent flow as the flow rate increases. The turbulent mixing of molecules produces eddy current which causes more interaction and frequent collision between the thermally energized liquid molecules. The thickness of thermal boundary layer at the tube wall decreases and heat exchange occurs directly between tube wall and bulk liquid phase without

Table 2
Simulated design variables obtained for single stage steam jet ejector using MS Excel in-built algorithms and mathematical functions

| Parameter | Magnitude |
|---|---|
| Vapour flow rate (kg/h) | 285 |
| Steam flow rate (kg/h) | 1,850 |
| Suction pressure (kg/cm$^2$ abs) | 0.06 |
| Discharge pressure (atm) | 1 |
| Nozzle throat area (m$^2$) | $3.38 \times 10^{-3}$ |
| Nozzle outlet area (m$^2$) | $8.39 \times 10^{-4}$ |
| Diffuser constant area (m$^2$) | 0.172 |

any boundary layer resistance. The transfer coefficient increases gradually for small scale thickness. For a scale thickness of 0.00005 m, the overall heat transfer coefficient gradually increases from 3,482.5 to 4,395.3 W/m$^2$ K. The increase in heat exchange coefficient is attributed to less resistance offered by small thickness of scale deposit. It was inferred that, as the scale thickness increases, the overall heat transfer coefficient decreases and the trend line makes negligible slope with horizontal reference axis. When the scale thickness is 0.0004 m the trend line almost resembles like a straight line parallel to horizontal axis. This means that the slope of the trend curve is zero which indicates that the overall heat transfer coefficient remains constant even though the volumetric flow rate increases for a large scale thickness. The presence of dirt and dissolved salts in water is responsible for fouling of tube interiors and development of scales. From the observed results it is concluded that as the scale thickness increases, the overall heat transfer coefficient decreases. It is due to the thermal resistance offered by scale deposit and temperature drop across the scale layer increases.

Fig. 5 analyzes the influence of scale thickness on overall heat transfer coefficient for a fixed flow rate of 1,500 m$^3$/h. It is elucidated from the trend curve that as scale thickness increases, the overall heat transfer coefficient decreases. The reason is attributed to the thermal conducting ability of scale substances. Since they are mainly produced from dissolved salts, the scale layers have poor thermal conductivity and rate of heat exchanged through

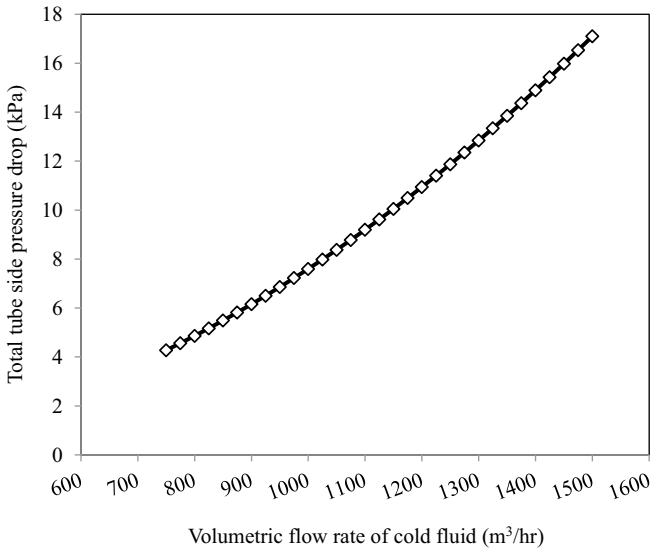


Fig. 3. Total tube side pressure drop expressed as function of volumetric flow rate of cold fluid.

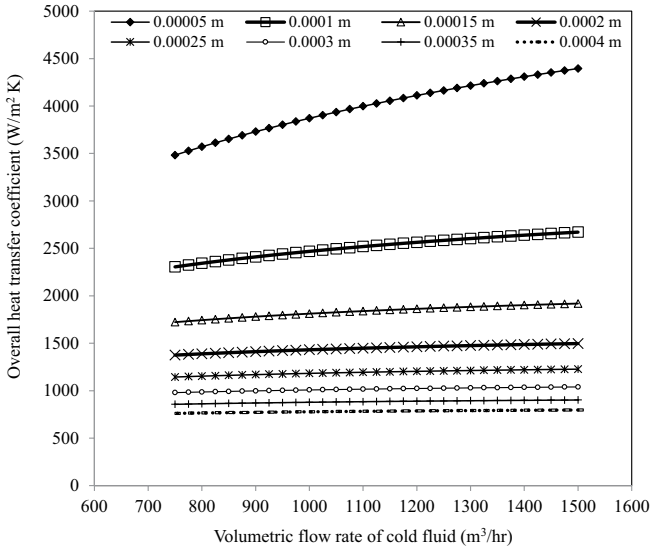


Fig. 4. Volumetric flow rate of cold fluid affecting overall heat transfer coefficient at different scale thickness.

the layer is very less. This causes a large temperature drop across the layer which decreases the overall heat exchange coefficient. This is in compliance with the standard statement; the overall heat transfer coefficient varies inversely with temperature drop. Due to scale deposits, the thermal resistance increases due to which the heat flux across the tube and scale decreases. The effect of scale thickness on percentage reduction in overall heat transfer coefficient is reported in Fig. 6. From the trend, it is concluded that the percentage reduction increases steeply for small variation in scale thickness. Almost 78.4% of response variable is attained within a short range of scale thickness 0–0.001 m. For larger scale thickness, the variation is less significant as the trend curve resembles like a straight line parallel to *x*-axis. When the scale thickness increases

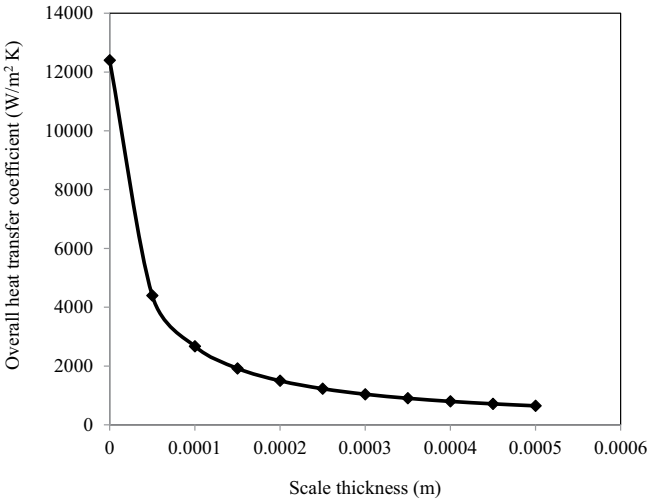


Fig. 5. Effect of scale thickness on overall heat transfer coefficient.

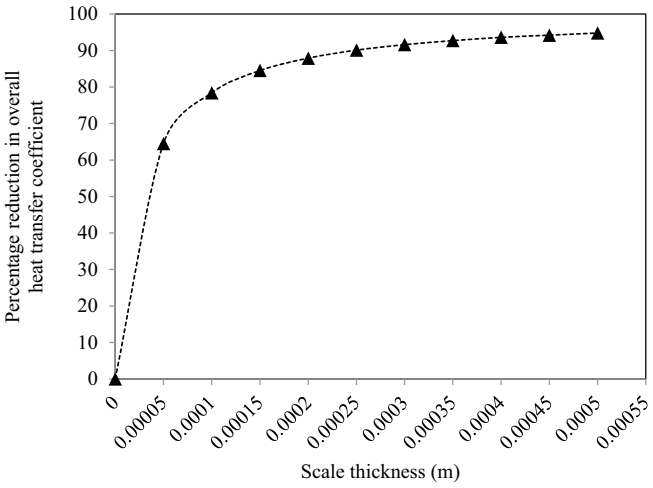


Fig. 6. Functional relationship between scale thickness and percentage reduction in overall heat transfer coefficient.

from 0.0002 to 0.0005 m, the percentage reduction rises meagerly from 87.9% to 94.8%. This concludes that large scale thickness is not having significant influence on percentage reduction in overall heat transfer coefficient.

In Fig. 7, the simultaneous effect of scale thickness and volumetric flow rate of brine solution on overall heat transfer coefficient is reported. The overall heat transfer coefficient decreases as scale thickness increases for various volumetric flow rates. At higher flow rate and for small scale thickness, the decrease is rapid whereas for large scale thickness the overall heat transfer coefficient almost attenuated and reached a plateau. The decreasing trend is due to the thermal resistance offered by scale material. A thick scale offers more thermal resistance rather than scale having less thickness. The functional relationship between brine flow rate and steam flow rate is reported in Fig. 8. The steam flow rate varies randomly with respect to input flow rate of brine solution. But when a trend line is drawn through the points predicted using

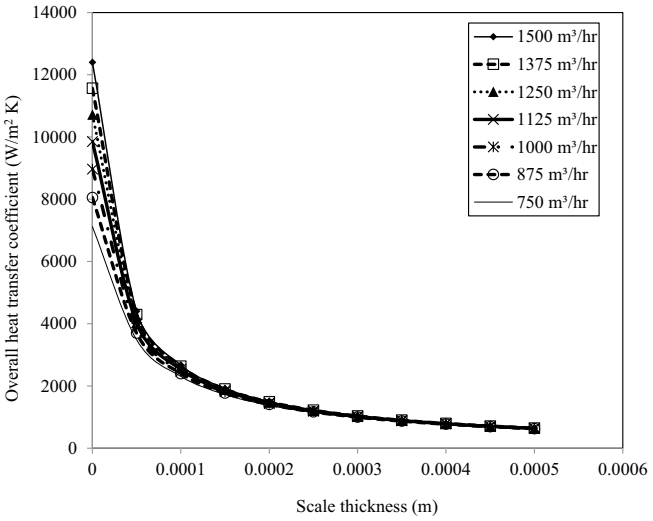


Fig. 7. Simultaneous effects of scale thickness and volumetric flow rate on overall heat transfer coefficient.

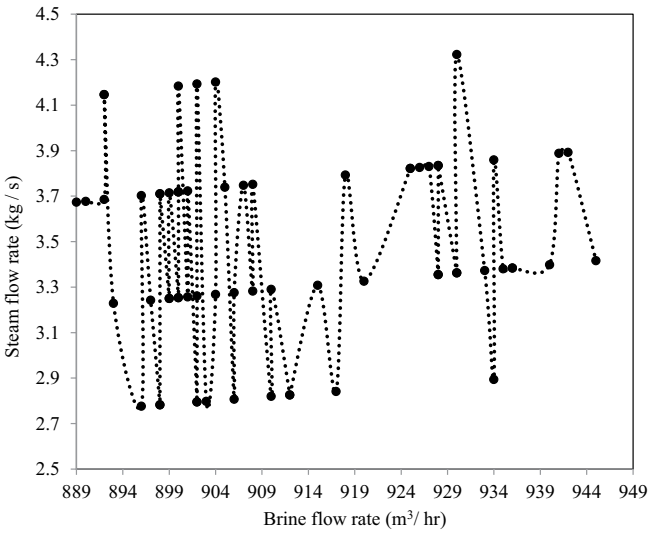


Fig. 8. Influence of brine flow rate on steam flow rate.

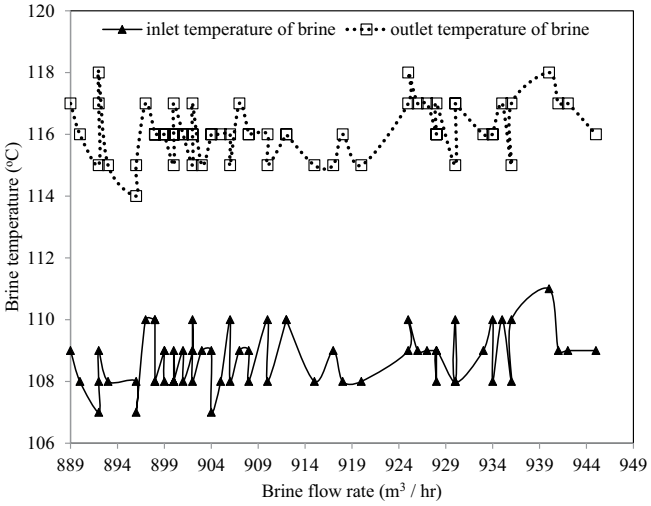


Fig. 9. Effect of brine flow rate on brine temperature.

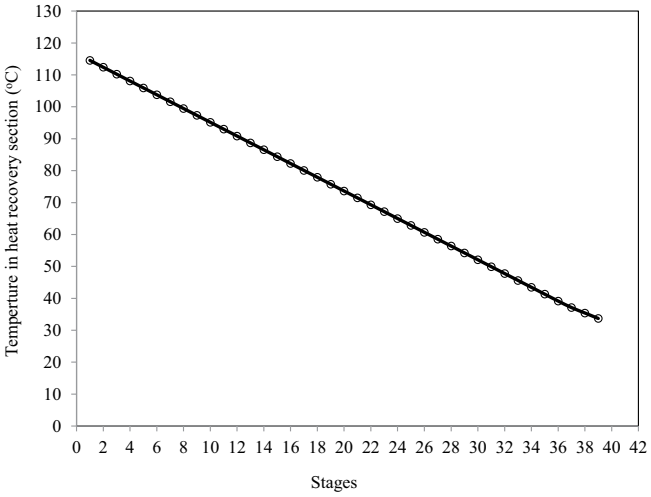


Fig. 10. Temperature in heat recovery section affected by stages.

least square principle, the steam flow rate increased with respect to increase in brine flow rate. The average of response variable is 3.467 kg/s. The maximum value of dependent variable is 4.323 kg/s and the minimum value is 2.776 kg/s. The range of the output variable is 1.547 kg/s. The trend pattern shows that the data points are distributed equally above and below the average value.

The effect of brine flow rate on brine temperature is depicted in Fig. 9. It was observed that both inlet and outlet temperature of brine varies randomly with respect to brine flow rate. The average temperature reached by brine solution at the outlet is 116.1°C. The maximum temperature attained at outlet is 118°C and minimum temperature attained is 114°C. The random variation in outlet temperature is due to sudden change in pressure in each stage of MSF unit and flow velocity of inlet brine solution. Fig. 10 expresses the variation of temperature in heat recovery section as function of stage number. It was observed that the variables temperature in recovery section and stage number is inversely related. As the stage number increases, the temperature in heat recovery section decreases linearly. This is attributed to the loss of enthalpy by process streams in the initial stages. The low temperature at the last stage is maintained because the feed water carries away the latent heat of the condensed steam. As the fresh hot brine enters the stages an equal amount of steam is formed as the pressure in the chamber remains constant. At the last stage, the brine and condensate temperature is almost same as the ambient temperature. Fig. 11 depicts the influence of stage number on mass flow rate of product. A linear decrease in trend was observed between the variables. The mass flow rate of product decreased as the stage number increases. The brine which enters heat recovery section initially absorbs latent heat of condensing vapors and then latent heat of steam. The heated brine introduced into the first stage flashes off and produces

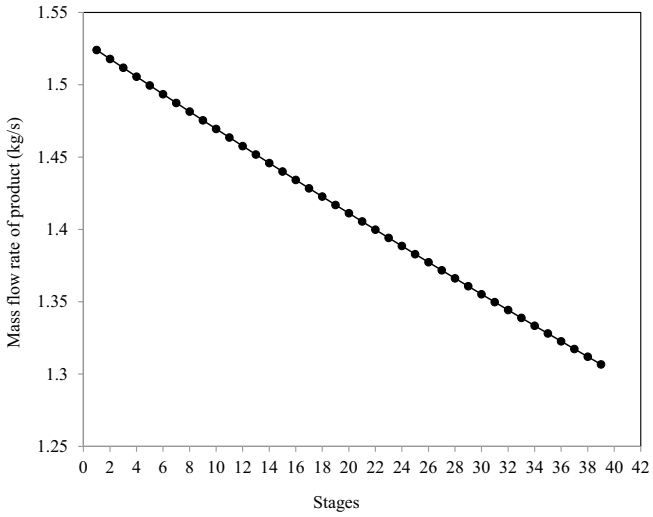


Fig. 11. Effect of stages on mass flow rate of product.

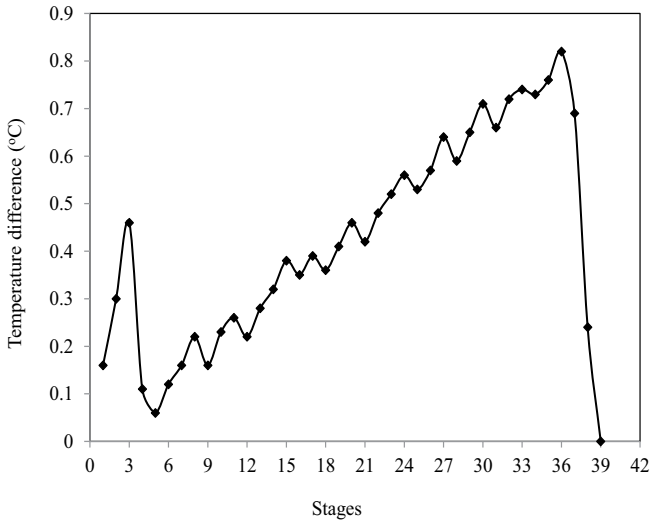


Fig. 12. Temperature difference between actual and theoretical expressed as function of stages.

condensed form of distillate. The enthalpy needed to flash off the brine solution decreases from stage to stage and this accounts for decrease in mass flow rate of products at the last stage. The variation of temperature difference with respect to stage number is reported in Fig. 12. It was inferred that as the stage number increases, the temperature difference increases first, reach a peak value and then decreases. The similar pattern is continued for higher stage numbers also. The average temperature difference was found to be 0.421°C.

## 6. Conclusions

The performance of brine heater and steam jet ejector used at NDDP Kalpakkam was analyzed. The influence of major variables on brine heater design and operation is studied. The effect of volumetric flow rate of brine on tube side pressure drop and overall heat transfer coefficient was studied. It is inferred that the tube side pressure drop increases continuously as function of volumetric flow rate and also the overall heat transfer coefficient increases with respect to volumetric flow rate. The overall heat transfer coefficient remained constant for a scale thickness of 0.0004 m even though the volumetric flow is increased. At this condition, the average heat transfer coefficient obtained was 781.97 W/m$^2$ K. The scale thickness had a significant influence on the rate of heat exchange and enthalpy loss in streams. The overall heat transfer coefficient decreased as the scale thickness increased from 0.0001 to 0.0005 m. But the scale thickness seems to have prudent influence on percentage reduction in overall heat exchanger coefficient. The rapid increase was observed for small change in scale thickness (0–0.00005 m) whereas the response variable does not change much for large change in scale thickness (0.00005–0.00055 m). This study concludes that the brine heater designed based on Kern method is efficient for utilizing in MSF unit and steam jet ejector output is comparable to that of the actual plant data.

## Symbols

| | | |
|---|---|---|
| $A$ | — | Heat exchange area, m$^2$ |
| $C_P$ | — | Heat capacity at constant pressure, J/(kg K) |
| $d_o$ | — | Outside diameter of tube, m |
| $d_i$ | — | Inside diameter of tube, m |
| $D_e$ | — | Equivalent diameter of shell side, m |
| $f$ | — | Tube side friction factor |
| $h_s$ | — | Shell side heat transfer coefficient, W/m$^2$ K |
| $K$ | — | Thermal conductivity of tube material, W/m K |
| $L$ | — | Length of tube, m |
| LMTD | — | Log mean temperature difference, K |
| $m$ | — | Mass flow rate of brine, kg/s |
| $M_d$ | — | Mass flow rate of distillate produced, kg/s |
| $n$ | — | Number of stages |
| $n_t$ | — | Number of tubes |
| $n_p$ | — | Number of tube passes |
| $P$ | — | Saturation pressure, kPa |
| $\Delta P_f$ | — | Pressure drop due to friction, N/m$^2$ |
| $Q$ | — | Heat duty of brine heater, J/s |
| $\Delta T$ | — | Temperature difference of brine solution, K |
| $U$ | — | Overall heat transfer coefficient, W/m$^2$ K |
| $V_t$ | — | Velocity of tube side fluid, m/s |
| $x_w$ | — | Tube wall thickness, m |

## Greek

| | | |
|---|---|---|
| $\rho_t$ | — | Density of tube side fluid, kg/m$^3$ |
| $\gamma$ | — | Isentropic expansion coefficient |
| $\eta_n$ | — | Nozzle efficiency |

## Subscripts

| | | |
|---|---|---|
| $f$ | — | Friction related variable |
| $s$ | — | Shell side fluid conditions |
| $e$ | — | Entrained vapor flow rate |
| $p$ | — | Motive steam flow rate |
| $c$ | — | Compressed vapor flow |

## References


[1] A.M.K. El-Ghonemy, Performance test of a sea water multi-stage flash distillation plant: case study, Alexandria Eng. J., 57 (2018) 2401–2413.

[2] H. Baig, M.A. Antar, S.M. Zubair, Performance evaluation of a once-through multi-stage flash distillation system: impact of brine heater fouling, Energy Convers. Manage., 52 (2011) 1414–1425.

[3] B. Masoumpour, M. Ataeizadeh, H. Hajabdollahi, M.S. Dehaj, Performance evaluation of a shell and tube heat exchanger with recovery of mass flow rate, J. Taiwan Inst. Chem. Eng., 123 (2021) 153–165.

[4] X. Li, L. Wang, R. Feng, Z. Wang, S. Liu, D. Zhu, Study on shell side heat transport enhancement of double tube heat exchangers by twisted oval tubes, Int. Commun. Heat Mass Transfer, 124 (2021) 105273, doi: 10.1016/j.icheatmasstransfer.2021.105273.

[5] Z. Yang, Y. Ma, N. Zhang, R. Smith, Design optimization of shell and tube heat exchangers sizing with heat transfer enhancement, Comput. Chem. Eng., 137 (2020) 106821, doi: 10.1016/j.compchemeng.2020.106821.

[6] J. Li, Z. Yang, S. Hu, F. Yang, Y. Duan, Effects of shell-and-tube heat exchanger arranged forms on the thermo-economic performance of organic Rankine cycle systems using hydrocarbons, Energy Convers. Manage., 203 (2020) 112248, doi: 10.1016/j.enconman.2019.112248.

[7] M.H. Mohammadi, H.R. Abbasi, A. Yavarinasab, H. Pourrahmani, Thermal optimization of shell and tube heat exchanger using porous baffles, Appl. Therm. Eng., 170 (2020) 115005, doi: 10.1016/j.applthermaleng.2020.115005.

[8] H. El-Dessouky, H. Ettouney, I. Alatiqi, G. Al-Nuwaibit, Evaluation of steam jet ejectors, Chem. Eng. Process., 41 (2002) 551–561.

[9] K. Zhang, X. Zhu, X. Ren, Q. Qiu, S. Shen, Numerical investigation on the effect of nozzle position for design of high performance ejector, Appl. Therm. Eng., 126 (2017) 594–601.

[10] H. Wu, Z. Liu, B. Han, Y. Li, Numerical investigation of the influences of mixing chamber geometries on steam ejector performance, Desalination, 353 (2014) 15–20.

[11] N. Sharifi, M. Sharifi, Reducing energy consumption of a steam ejector through experimental optimization of the nozzle geometry, Energy, 66 (2014) 860–867.

[12] K. Ariafar, D. Buttsworth, N. Sharifi, R. Malpress, Ejector primary nozzle steam condensation: area ratio effects and mixing layer development, Appl. Therm. Eng., 71 (2014) 519–527.

[13] S. Varga, A.C. Oliveira, B. Diaconu, Influence of geometrical factors on steam ejector performance – a numerical assessment, Int. J. Refrig., 32 (2009) 1694–1701.

[14] J.G. del Valle, J.M. Sáiz Jabardo, F.C. Ruiz, A one dimensional model for the determination of an ejector entrainment ratio, Int. J. Refrig., 35 (2012) 772–784.

[15] A.N.A. Mabrouk, Technoeconomic analysis of once through long tube MSF process for high capacity desalination plants, Desalination, 317 (2013) 84–94.

[16] A. Sellami, M.B. Ali, M. Lakhdar, L. Kairouani, Once-through multistage flash desalination installation combined with thermal vapour compression MSF-OT/TVC, Desal. Water Treat., 161 (2019) 48–55.

[17] S. Wuryanti, Design of MSF type brine circulation system for steam power plant, J. Phys.: Conf. Ser., 1450 (2020) 1–7.

[18] H. El-Dessouky, H.I. Shaban, H. Al-Ramadan, Multi-stage flash desalination process: a thermal analysis, Dev. Chem. Eng. Min. Process., 4 (1996) 5–22.

[19] A.J. Toth, Modelling and optimisation of multi-stage flash distillation and reverse osmosis for desalination of saline process wastewater sources, Membranes, 10 (2020) 1–18.

[20] S. Draggan, J. Dionne, H. Mahar, F. Brier, Initial Environmental Evaluation Replacement of the Seawater Desalination System, McMurdo Station, Antartica, National Science Foundation, Washington DC, 1993.

[21] I. Khoshrou, M.R.J. Nasr, K. Bakhtari, New opportunities in mass and energy consumption of the multi-stage flash distillation type of brackish water desalination process, Sol. Energy, 153 (2017) 115–125.

[22] M. Assiri, M.A. Antar, O. Hamed, D.U. Lawal, Performance improvement of multi-stage flash desalination with thermal vapor compression, a practical consideration, Int. J. Energy Res., 45 (2021) 20651–20671.

[23] H. El-Dessouky, H. Ettouney, I. Alatiqi, G. Al-Nuwaibit, Evaluation of steam jet ejectors, Chem. Eng. Process. Process Intensif., 41(2002) 551–561.